FOURTH INTERIM TOPICAL REPORT

on

A STUDY OF THE MECHANICS OF CLOSED-DIE FORGING

FORGING LOADS AND STRESSES IN CLOSED-DIE FORGING PART TWO

to

ARMY MATERIAL AND
MECHANICS RESEARCH CENTER

April 30, 1969

by

T. Altan, H. J. Henning, and A. M. Sabroff

Contract DAAG46-68-C-0111

BATTELLE MEMORIAL INSTITUTE
Columbus Laboratories
505 King Avenue
Columbus, Ohio 43201

FOURTH INTERIM TOPICAL REPORT

on

A STUDY OF THE MECHANICS OF CLOSED-DIE FORGING

FORGING LOADS AND STRESSES IN CLOSED-DIE FORGING PART TWO

to

ARMY MATERIAL AND
MECHANICS RESEARCH CENTER

April 30, 1969

by

T. Altan, H. J. Henning, and A. M. Sabroff

Contract DAAG46-68-C-0111

BATTELLE MEMORIAL INSTITUTE
Columbus Laboratories
505 King Avenue
Columbus, Ohio 43201

FOREWORD

This topical report on "Forging Loads and Stresses in Closed-Die Forging, Part Two" covers the analytical work performed under Contract No. DAAG46-68-C-0111 with Battelle Memorial Institute of Columbus, Ohio, from December 30, 1968, to March 15, 1969.

This work was administered under the technical direction of Mr. Robert M. Colton and Mr. Dennis Green of the Army Materials and Mechanics Research Center, Watertown, Massachusetts 02172.

This program was carried out under the supervision of Mr. A. M. Sabroff, Chief of the Metalworking Division, and Mr. H. J. Henning, Associate Chief of the Metalworking Division. Dr. T. Altan, Senior Scientist, is the principal investigator.

TABLE OF CONTENTS

FORGING LOADS AND STRESSES IN CLOSED-DIE FORGING PART TWO

by

T. Altan, H. J. Henning, and A. M. Sabroff

ABSTRACT

The slab method of analysis for predicting forging stresses and loads has been applied to longitudinal (axial) flow, i.e., to extrusion-type forging. Both plane strain and axisymmetric deformations were considered. The flow models, already discussed in the Third Interim Topical Report, have been further studied, and the necessary equations for general use are derived. The flash-line location has been shown to have little effect upon maximum forging load if die-cooling effects are not too large. The present study, along with the Third Interim Topical Report, represents a fundamental method for obtaining detailed information on the mechanics of closed-die forging.

INTRODUCTION

During most closed-die forging operations, the metal being forged flows in several directions, depending on the geometry of the dies. At the outset of deformation, the metal flows most readily in the lateral direction until it meets enough obstruction(s) to cause it to flow into the longitudinally (axially) oriented cavities that might be in the die(s). If all of the horizontal avenues of escape are essentially blocked off, the metal is forced to fill completely the longitudinal cavities. Increased friction can also restrict lateral flow and promote longitudinal flow. Stated more technically, whenever the energy necessary for lateral flow is larger than the energy necessary to promote longitudinal (or axial) flow, the latter takes place and the die cavities start to fill.

The flash gap usually represents the most important obstruction to lateral flow. Thus, the design of the flash geometry plays an important role in controlling forging energy and in promoting die filling.

In the Third Interim Topical Report on "Forging Loads and Stresses in Closed Dies – Part One", the lateral flow and die stresses occurring in closed-die forging were analyzed particularly for forging in dies having a generally flat configuration (having little or no longitudinal metal movement). This topical report is concerned with analyses of flow and stress occurring while forging with dies having deeper, longitudinally oriented cavities.

Together the two topical reports present a series of analyses useful for estimating the flow and stresses in forging of more complex shapes. A Fifth Interim Topical Report is being prepared to demonstrate how these analyses can be applied to practical forgings.

While the derivations presented here require some extensive calculations, the final analytical procedures developed are quite straightforward. Nevertheless, the use of computers would be useful when applying the analytical procedures in day-to-day operations.

GENERAL DERIVATIONS OF STRESS DISTRIBUTION AND AVERAGE FORGING PRESSURE REQUIRED IN EXTRUSION-TYPE, LONGITUDINAL FLOW

It is quite clear that there are no simple analyses applicable to the myriad of shapes being forged everyday. However, when the most complicated shape is viewed as being comprised of several connected components, each having a characteristic metal-flow behavior, the analyses become more rational. The majority of forging shapes comprise one or more of the following basic situations in each of the connected components:

(1) Plane-strain, lateral flow

(2) Axisymmetric, lateral flow

(3) Plane-strain, longitudinal (axial) flow

(4) Axisymmetric, longitudinal flow.

The total load required for forging any part is then a summation of the loads required for each component. The sections that follow are concerned mainly with the derivations of analyses for those components of forgings involving longitudinal flow.

Plane-Strain, Longitudinal Flow

Figure 1 contains two sketches to illustrate plane-strain deformation with longitudinal (axial) flow. The arrows in the upper sketch show generally how metal flows both laterally and longitudinally (axially) in a rib-type die arrangement. The cross-sectional view is taken through a long rib extruding front to back with respect to the page. The metal flows into the vertical rib cavity as the dies close. The lower sketch in Figure 1 shows the various symbols for expressing die geometry and stresses active in the forging of such a rib. It should be emphasized here that the rib is considered to be large enough that all of the metal flow is considered to be in the plane of the page.

In the derivation for this plane-strain situation, it is assumed that the metal is in static equilibrium under pressure from the downward force of the ram. In this case, the metal flows laterally inward and outward on either side of the two "neutral surfaces" located in the web of the forging (illustrated in the upper sketch of Figure 1). The significance of these neutral surfaces as they relate to the analyses of metal flow will be discussed in a later section.

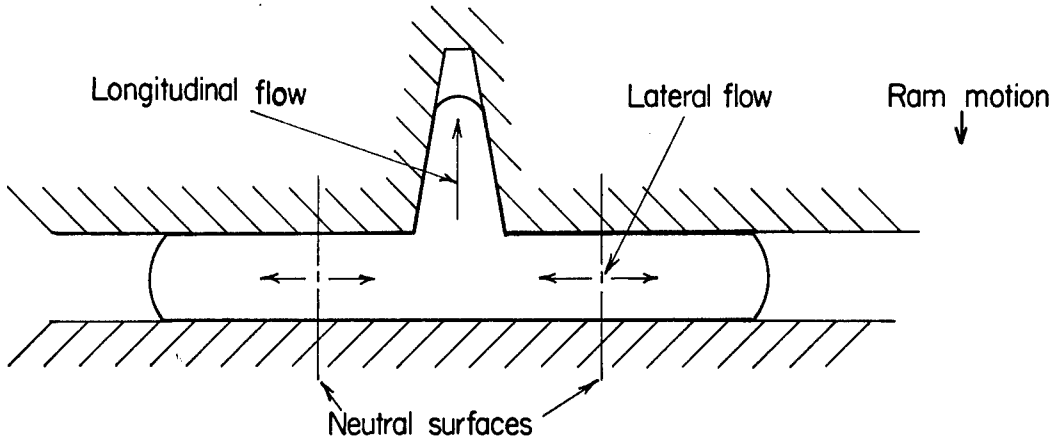

a. Example of Plane-Strain, Longitudinal Flow

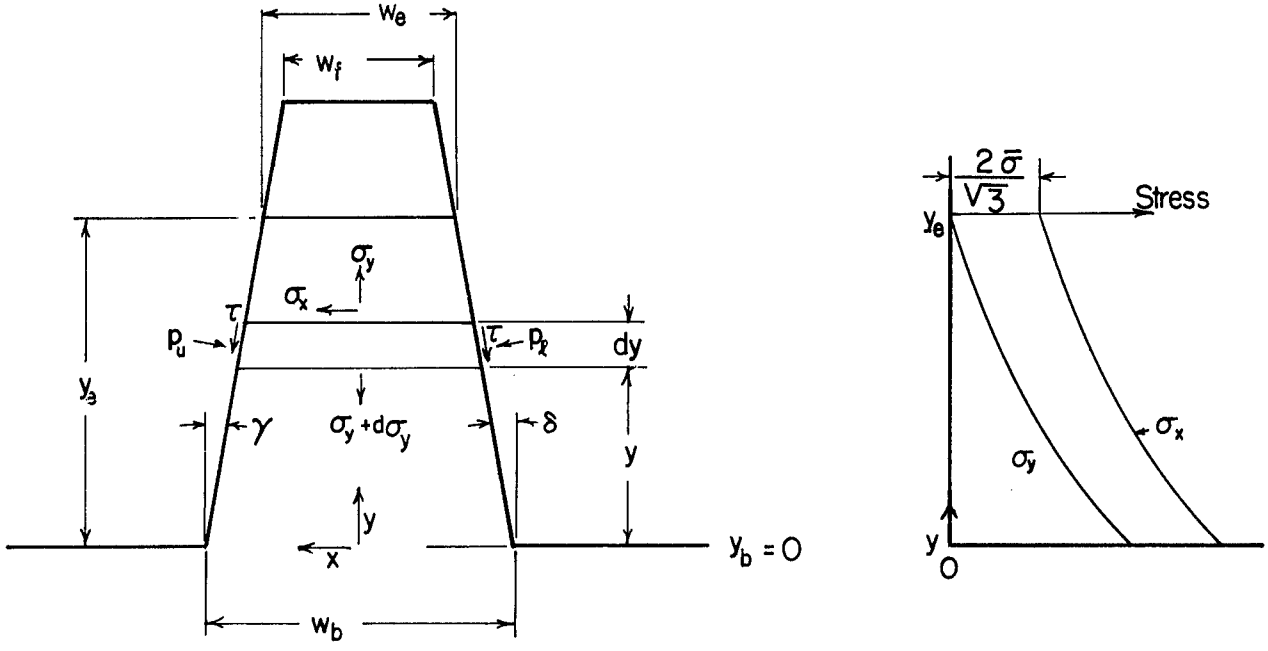

b. Analytical Model of Plane-Strain, Longitudinal Flow and the Typical Stress Distribution

FIGURE 1. ILLUSTRATION OF AN ANALYTICAL MODEL OF PLANE-STRAIN LONGITUDINAL FLOW OCCURRING IN FORGING

Following Figure 1, from the static equilibrium the following relations are obtained:

The lateral pressures acting on the cavity walls*

$$p_u = \sigma_x + \tau \tan \gamma \tag{1}$$

$$p_\ell = \sigma_x + \tau \tan \delta \, . \tag{2}$$

The lateral stress distribution

$$\sigma_x = \frac{K_2}{K_1} \ln \left(\frac{w_e}{w_b + K_1 y} \right) + \sigma_{xe} \, , \tag{3}$$

where

$$w_e = w_b + K_1 y_e \tag{4}$$

$$K_1 = - (\tan \gamma + \tan \delta) \tag{5}$$

$$K_2 = \frac{2}{\sqrt{3}} \bar{\sigma} K_1 + \tau (2 + \tan^2 \gamma + \tan^2 \delta). \tag{6}$$

The flow rules applied to the coordinates of Figure 1 give

$$\sigma_y = \sigma_x - \frac{2}{\sqrt{3}} \bar{\sigma} \, . \tag{7}$$

Equations (3) through (7) illustrate that the lateral stress, σ_x, and the longitudinal stress, σ_y, increase with increasing depth of fill y, with friction shear stress, τ, and with increasing draft of the cavity, i.e., with increasing draft angles γ and δ.

It should be noted that if the cavity is not completely filled, i.e., for $\sigma_{ye} = 0$ at $y = y_e$, the stress in lateral direction is determined from the flow rule to be as follows:

$$\sigma_{xe} = + \frac{2}{\sqrt{3}} \bar{\sigma} + \sigma_{ye} \text{ at } y = y_e \, . \tag{8}$$

At the point where the cavity is just filled, (i.e., $w_e = w_f$ in Figure 1) the longitudinal stress, σ_{ye}, begins to be larger than 0. Here is the point where the analysis can begin to introduce error by estimating values for σ_y that are too low.

*Symbols are listed at the end of this report.

The forming load per unit depth in the direction of the ram motion is given for y = 0:

$$P = w_b \sigma_y \ (y = 0). \tag{9}$$

Thus, the forging load is obtained from Equations (7), (3), and (9):

$$P = w_b \left[\frac{K_2}{K_1} \ln \left(\frac{w_e}{w_b} \right) + \sigma_{xe} - \frac{2}{\sqrt{3}} \bar{\sigma} \right]. \tag{10}$$

To evaluate Equation (10), the values of w_e, K_1, and K_2 must be calculated from Equations (4), (5), and (6), respectively. This represents a rather lengthy series of calculations for a rib having a draft or taper.

The analysis can be simplified somewhat by assuming that the walls of the cavity are not tapered. In this case

the draft angles $\gamma = \delta = 0$,

the rib widths $w_b = w_e = w_f = w$,

and the wall pressures $p_u = p = \sigma_x$.

The lateral stress distribution is given by

$$\sigma_x = - \frac{2\tau}{w} y + \sigma_{xe} \ . \tag{11}$$

The forming load per unit depth at y = 0 is given by

$$P = w \sigma_y \ (y = 0) = w \frac{2\tau}{w} y_e = 2\tau y_e \ . \tag{12}$$

The forging load increases linearly with the friction shear stress, τ, and the filled cavity of depth, y_e. In cases where the die cavity walls are both tilted in the same direction, yet tapered towards each other, the Equations (3) and (10) are still valid for calculating the lateral stress distribution and the forging load. The appropriate signs, however, must be used with the draft angles γ and δ, which are considered as positive for the directions shown in Figure 1.

The forgoing derivations can be applied to the task of estimating the forces in forging of long parts having ribs. In such cases, the metal flow is predominantly in a given plane transverse to the center line of the rib except near the ends of the part where the metal tends to flow along the rib cavity as well. This is where the metal is flowing more radially, similar to that occurring in axisymmetric dies.

Axisymmetric Longitudinal Flow in an Annular Rib

Figure 2 contains two sketches to illustrate the directions of metal flow in the forging of a disk having an annular rib. In the upper sketch, the arrows show in general how the metal flows both radially and longitudinally (axially) in a die arrangement typically used for forging turbine components. The lower sketch in Figure 2, shows the various symbols for expressing die geometry and stresses active in forging such a part.

Similar to the previous examples, it is assumed in this derivation that the metal is in static equilibrium under pressure from the downward force of the ram.

Following Figure 2, the equilibrium in axial z direction yields the following:

$$- (\sigma_z + d\sigma_z) \left[(r_o + dr_o)^2 - (r_i + dr_i)^2 \right] \pi + \sigma_z (r_o^2 - r_i^2) \pi$$

$$- \tau \frac{dz}{\cos \gamma} \cdot \cos \gamma \, 2\pi \left(r_i + \frac{dr_i}{2} \right) - \tau \frac{dz}{\cos \delta} \cdot \cos \delta \, 2\pi \left(r_o + \frac{dr_o}{2} \right)$$

$$- p_i \frac{dz}{\cos \gamma} \cdot \sin \gamma \, 2\pi \left(r_i + \frac{dr_i}{2} \right) - p_o \frac{dz}{\cos \delta} \cdot \sin \delta \, 2\pi \left(r_o + \frac{dr_o}{2} \right) = 0 . \qquad (13a)$$

The subscripts i and o refer to inside and outside surfaces, respectively. By neglecting high order differentials and after simplifying, Equation (13a) results in:

$$+ \sigma_z (2 r_i dr_i - 2 r_o dr_o) + d\sigma_z (r_i^2 - r_o^2) - 2\tau dz (r_i + r_o)$$

$$- 2p_i dz \tan \gamma \, r_i - 2p_o dz \, r_o \tan \delta = 0. \qquad (13b)$$

In a similar manner, the equilibrium in radial direction gives, Figure 2,

$$p_i = \sigma_r + \tau \tan \gamma \qquad (14a)$$

$$p_o = \sigma_r + \tau \tan \delta . \qquad (14b)$$

From Figure 2 it is seen that

$$r_i = r_{ib} + z \tan \gamma \text{ and } dr_i = dz \tan \gamma \qquad (15a)$$

$$r_o = r_{ob} - z \tan \delta \text{ and } dr_o = - dz \tan \delta . \qquad (15b)$$

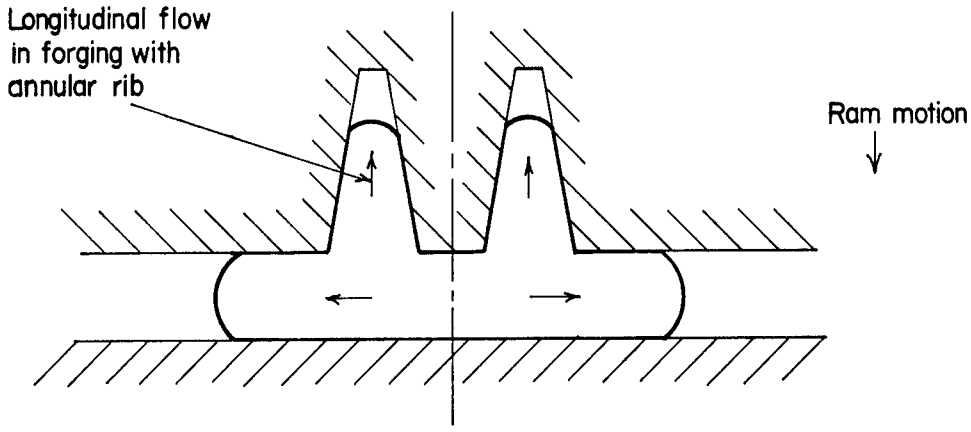

a. Example of Axisymmetric Forging With Annular Rib

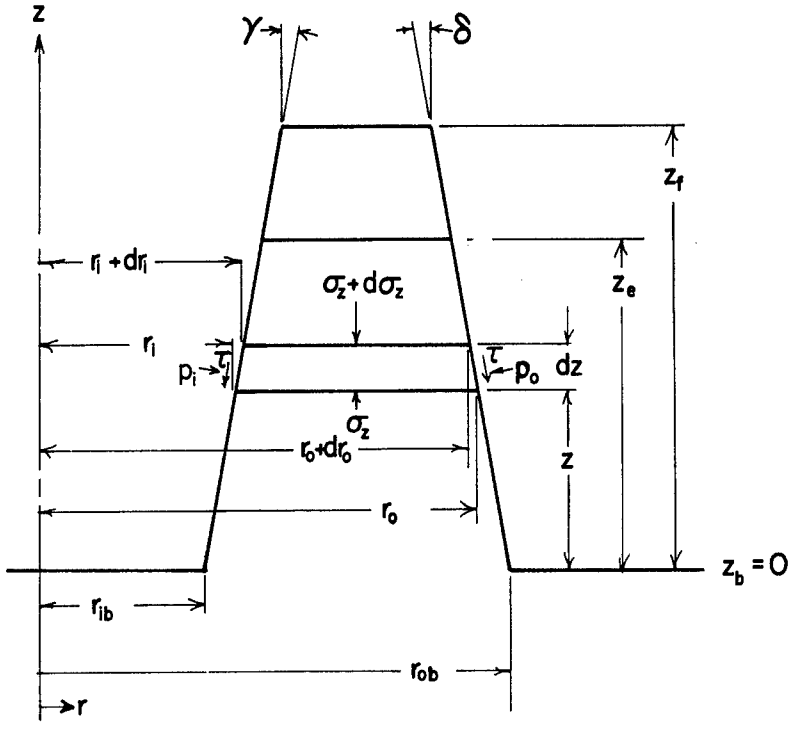

b. Analytical Model of Axisymmetric Longitudinal flow

FIGURE 2. ILLUSTRATION OF AN ANALYTICAL MODEL FOR LONGITUDINAL FLOW IN AN AXISYMMETRIC DIE HAVING AN ANNULAR RIB

The substitution of Equations (14a), (14b), (15a), and (15b) into Equation (13b) results in the following differential equation:

$$-\frac{d\sigma_z}{dz}\left(C z^2 + Bz + A\right) + zD + E = 0 \tag{16a}$$

or

$$\frac{d\sigma_z}{dz} = \frac{zD}{Cz^2 + 2Bz + A} + \frac{E}{Cz^2 + 2Bz + A}\ , \tag{16b}$$

where

$$A = r_{ob}^2 - r_{ib}^2 \tag{17a}$$

$$B = -\left(r_{ib} \tan\gamma + r_{ob} \tan\delta\right) \tag{17b}$$

$$C = \tan^2\delta - \tan^2\gamma \tag{17c}$$

$$D = 2\left(-C - \tau\frac{\tan\gamma}{\cos^2\gamma} + \tau\frac{\tan\delta}{\cos^2\delta}\right) \tag{17d}$$

$$E = 2\left(r_{ob}\tan\delta + r_{ib}\tan\gamma - r_{ib}\frac{\tau}{\cos^2\gamma} - r_{ob}\frac{\tau}{\cos^2\delta}\right), \tag{17e}$$

and introducing

$$F = \left(CA - B^2\right)^{1/2} = \left(r_{ib}\tan\gamma + r_{ob}\tan\delta\right). \tag{17f}$$

The integration of Equation (16b) results in:

$$\sigma_z = \frac{D}{2C}\ln\left(A + 2Bz + Cz^2\right) + \left(1 - \frac{DB}{C}\right)\frac{1}{2F}\ln\left|\frac{F - B - Cz}{F + B + Cz}\right| + I\ . \tag{18}$$

Equation (18) represents the axial-stress distribution inside the die cavity shown in Figure 2. The axial stress, σ_z, increases within the material itself from zero to its maximum value as the depth of fill, z, decreases from $z = z_b = 0$, shown in Figure 2. The subscripts b and e refer to beginning and end of the cavity depth, respectively. The axial stress, σ_z, at the rib entrance, $z = 0$, reaches its highest value when the rib is completely filled.

The symbol, I, in Equation (18) designates the integration constant, which is determined from the condition: $\sigma_z = 0$ at $z = z_e$, when the cavity is not completely filled. Thus, from Equation (18),

$$I = -\frac{D}{2C} \ln \left(A + 2Bz_e + Cz_e^2 \right) - \left(1 - \frac{DB}{C} \right) \frac{1}{2F} \ln \left| \frac{F - B - Cz_e}{F + B + Cz_e} \right| . \quad (19)$$

Using the yield condition $\sigma_r = \sigma_z + \overline{\sigma}$, and the Equations (14a) and (14b), the radial cavity pressures, p_i, and, p_o, can also be determined (referring to Figure 2).

The forming load at z = 0 is given by the following:

$$= \pi \left(r_{ob}^2 - r_{ib}^2 \right) \sigma_z \, (z = 0) , \quad (20)$$

where σ_z is obtained from Equations (18) and (19) for z = 0,

$$\sigma_z \, (z = 0) = \frac{D}{2C} \ln \left(\frac{A}{A + 2Bz_e + Cz_e^2} \right) + \left(1 - \frac{DB}{C} \right) \frac{1}{2F} \ln \left[\frac{(F - B)(F + B + Cz_e}{(F + B)(F - B - Cz_e)} \right] . \quad (21)$$

The above expressions, derived for calculating the stresses and the load in the forging of an annular rib, are considered to be too complicated for practical use, unless the calculations are carried out by a computer.

A reasonable approximation of forging loads can be obtained if the tapers, i.e., the draft angles, are neglected (shown in Figure 2). In this case, $\gamma = \delta = 0$, Equation (16e), is simplified to:

$$\frac{d\sigma_z}{dz} \left(r_o^2 - r_i^2 \right) + 2\tau \left(r_o + r_i \right) = 0 . \quad (22)$$

The solution of Equation (22) is as follows:

$$\sigma_z = \frac{2\tau}{r_o - r_i} \left(z_e - z \right) . \quad (23)$$

Equation (23) illustrates that the axial stress, σ_z, in the cavity (Figure 2), increases linearly from the top towards the bottom of the cavity. The axial stress, σ_z, is directly proportional to the friction stress, τ, and inversely proportional to thickness of the annular-rib cavity as expressed by $r_o - r_i$ (Figure 2).

Without considering the draft angles, the radial pressure acting on the cavity walls will be as follows:

$$p = \sigma_r = \sigma_z + \overline{\sigma} . \quad (24)$$

The forging load at z = 0 is

$$P = \pi \left(r_o^2 - r_i^2 \right) \quad \sigma_z \, (z = 0) = \pi \left(r_o + r_i \right) 2\tau \, z_e . \quad (25)$$

From this equation it is seen that neglecting the draft angles greatly simplifies the load calculation. These derivations apply, for example, to the analyses of flow and forces active in forging of a typical rib- and web-structural forging.

Axisymmetric Longitudinal Flow in a Central Shaft

Many aircraft and automotive-gear-type forgings are typically represented by the two sketches shown in Figure 3 which illustrates the directions of metal flow in the forging of such parts. In the upper sketch, the arrows show generally how the metal flows both radially and longitudinally (axially) in such a die arrangement. The lower sketch of Figure 3 shows the various symbols for expressing die geometry and stresses active in forging such a part.

In the derivation for this case, the metal was considered to be in static equilibrium under pressure from the downward force of the ram. The metal tends to flow out radially at first until it reaches enough resistance to cause it to flow into the shaft. Similar to the previous derivations, the equilibrium conditions are expressed for the axial state of stress as follows:

$$-(\sigma_z + d\sigma_z)(r + dr)^2\pi + \sigma_z \pi r^2 - \tau \frac{dz}{\cos\gamma} \cos\gamma \, 2\pi r$$

$$- \frac{dz}{\cos\gamma} \, p \sin\gamma \, 2\pi r = 0 \, . \qquad (26a)$$

For $\gamma = \delta$, r_b = radius of the shaft at $z = 0$.

After simplification and by neglecting the high order differentials, Equation (26a) transforms into

$$2\sigma_z dr + d\sigma_z \, r + 2\tau dz + 2dz \, p \tan\gamma = 0. \qquad (26b)$$

From the geometry of Figure 3,

$$dr = - dz \tan\gamma$$

$$r = r_b - z \tan\gamma .$$

Further, the equilibrium in r direction gives

$$p = \sigma_r + \tau \tan\gamma \ ,$$

or with the flow rule, $\sigma_r - \sigma_z = - \bar{\sigma}$,

$$p = \sigma_z - \bar{\sigma} + \tau \tan\gamma \ . \qquad (27)$$

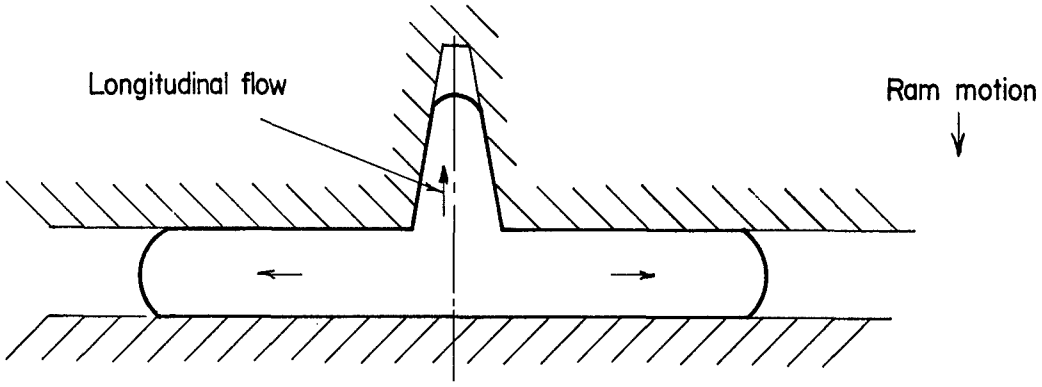

a. Example of Axisymmetric Forging With Central Shaft

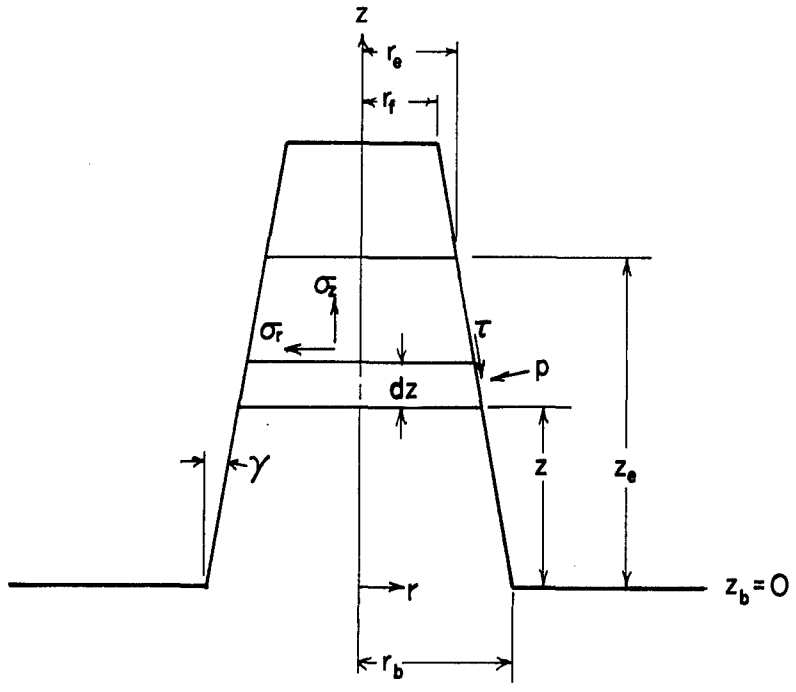

b. Analytical Model for Axisymmetric Longitudinal Flow

FIGURE 3. ILLUSTRATION OF AN ANALYTICAL MODEL FOR LONGITUDINAL FLOW IN AN AXISYMMETRIC DIE WITH A SHAFT AT THE CENTER

Substituting Equation (27) into Equation (26b) gives, after simplification,

$$\frac{d\sigma_z}{dz} = \frac{2\,\bar{\sigma}\tan\gamma - 2\tau\,(1 + \tan^2\gamma)}{(r_b - z\tan\gamma)} \quad . \tag{28}$$

The integration of Equation (28) with the consideration of the boundary condition gives,

$$\sigma_z = 2\,\frac{[\tau\,(1 + \tan^2\gamma) - \bar{\sigma}\tan\gamma]}{\tan\gamma} \ln\left(\frac{r_b - z\tan\gamma}{r_b - z_e\tan\gamma}\right) \quad . \tag{29}$$

Equation (29) describes the axial-stress distribution in the shaft, Figure 3. It is seen that, as expected, the axial stress, σ_z, increases with increasing draft angle, γ, and with decreasing depth of fill, z.

The forging load at z = 0 is

$$P = \pi r_b^2\,\sigma_z\,(z = 0)$$

$$= \pi r_b^2\,2\frac{[\tau\,(1 + \tan^2\gamma) - \sigma\tan\gamma]}{\tan\gamma} \ln\left(\frac{r_b}{r_b - z_e\tan\gamma}\right) \quad . \tag{30}$$

The stresses and the forging load given by Equations (28) and (30) will be greatly simplified if the taper of the shaft is neglected, i.e., $\gamma = 0$, $r_e = r_b$. In this case, the average thickness of the rib can be considered. The axial stress is then given by the following:

$$\sigma_z = \frac{2\tau}{r_b}\,(z_e - z) \quad . \tag{31}$$

The radial pressure is

$$p = \sigma_r = \sigma_z + \bar{\sigma} \quad , \tag{32}$$

and the forging load at z = 0 is

$$P = \pi r_b^2\,\frac{2\tau z_e}{r_b} = 2\pi r_b z_e \tau \quad . \tag{33}$$

DETERMINATION OF FLOW MODELS IN STEEP-SIDED DIE IMPRESSIONS

To complete the analysis so far, the analyses for states of stress in situations must also be considered where the die cavity is essentially filled, but the dies have not yet closed.

The determination of flow models representing metal flow into a smaller flash cavity in plane strain and in axisymmetric forgings with flash were discussed in the Third Interim Topical Report. In those cases studied, however, it was assumed that the lower and upper depths of the die cavity were large enough to permit the theoretical shear surfaces to form, i.e., in Figure 4 the following conditions hold:

$$\frac{h-t}{2} \leq h_u$$

and (34)

$$\frac{h-t}{2} < h_\ell \ .$$

The subscripts u and ℓ refer to upper and lower dies, respectively.

Flow Models for Formation of a Thin Flash

The discussion given below applies to plane strain as well as axisymmetric forging. When the forging is thin enough that the conditions (34) are not satisfied, the flow models seen in Figures 5a, 5b, and 5c might exist where the flash center line is not at the center of the total cavity depth. In cases of Figures 5a and 5b, the upper shear surfaces are free to form while the lower horizontal shear surface is essentially replaced by the die surface. For given die geometry, if it is assumed that the depth of the upper cavity is sufficiently large, the theoretical metal flow model will be one of the models described in Figures 5a and 5b. In the flow model of Figure 5c, the height, h, of the deformation zone is essentially determined by the die geometry.

In the flow models seen in Figures 5a and 5b, to calculate the stress distribution and the load with the equations given in the Third Interim Topical Report, the following parameters must be determined:

(a) Height of deformation zone, h

(b) Angle of upper shear surface, α

(c) Angle of lower shear surface, β.

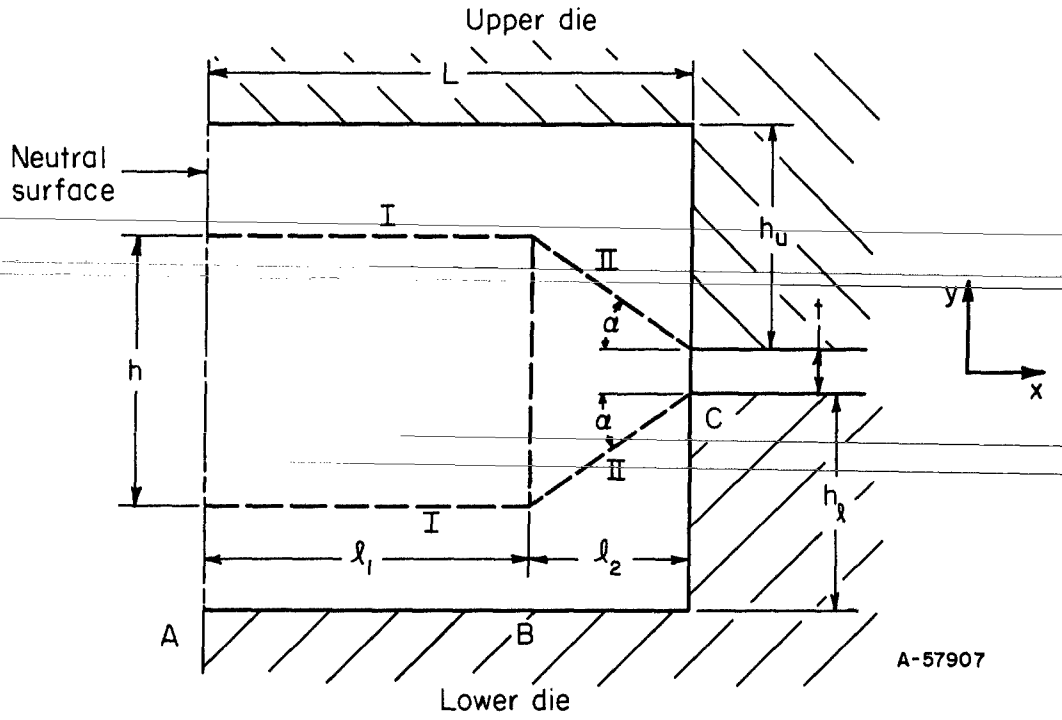

FIGURE 4. FLOW MODEL REPRESENTING METAL FLOW INTO FLASH (DIE CAVITY HAS SUFFICIENT DEPTH FOR THEORETICAL SHEAR SURFACES TO FORM)

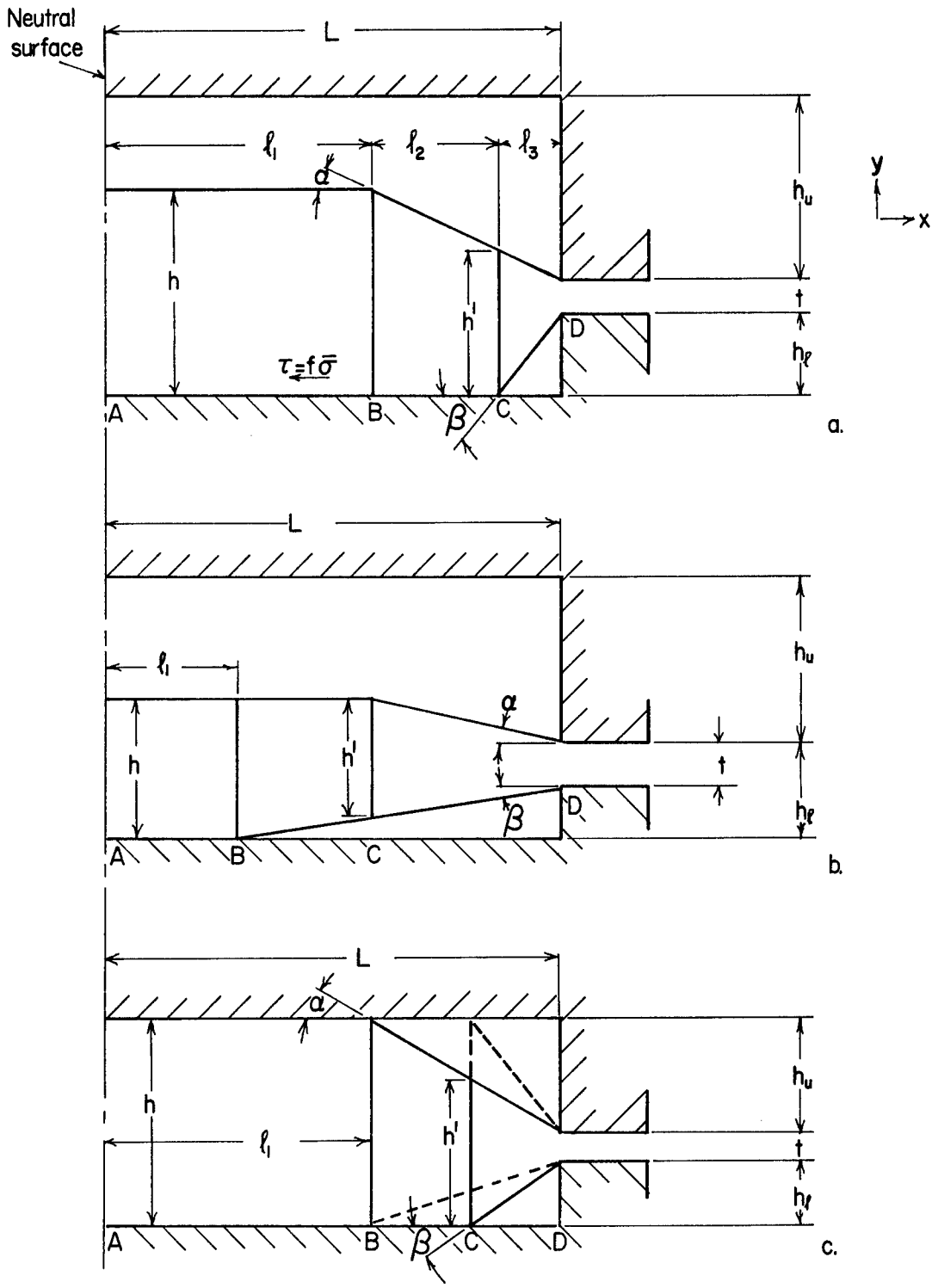

FIGURE 5. FLOW MODELS ILLUSTRATING POSSIBLE DEFORMATION ZONE WHEN FLASH IS NOT AT CENTER

(AXISYMMETRIC AND PLANE STRAIN)

Following Figure 5a and using the derivations given in the Third Interim Topical Report, the longitudinal stress at the neutral surface, A, is,

$$\sigma_{yA} = \frac{K_2}{K_1} \ln \frac{t}{h'} + \frac{C_2}{C_1} \ln \frac{h'}{h} + \frac{\ell_1}{h} \left(\frac{\bar{\sigma}}{\sqrt{3}} + \tau \right) + \sigma_{yD} \quad , \tag{35}$$

where

σ_{yD} = longitudinal stress at plane D, independent of the parameters h, α, and β

$$K_1 = - (\tan \alpha + \tan \beta) \tag{36}$$

$$K_2 = - \frac{2}{\sqrt{3}} \bar{\sigma} K_1 + \frac{\bar{\sigma}}{\sqrt{3}} (2 + \tan^2 \alpha + \tan^2 \beta) \tag{37}$$

$$C_1 = - \tan \alpha \tag{38}$$

$$C_2 = \frac{2}{\sqrt{3}} \bar{\sigma} \tan \alpha + \tau + \frac{\bar{\sigma}}{\sqrt{3}} (1 + \tan^2 \alpha) \tag{39}$$

$$\tau = f\bar{\sigma}, \text{ friction shear stress with } 0 \leq f \leq 0.577 \quad , \tag{40}$$

and from the geometry of Figure (5a),

$$h' = t + \frac{h_\ell}{\tan \beta} (\tan \alpha + \tan \beta) \tag{41}$$

$$\ell_1 = L - \frac{(h - h')}{\tan \alpha} - \frac{h_\ell}{\tan \beta} \quad . \tag{42}$$

Following the flow model described in Figure 5b, the stress, σ_{yA}, at the plane, A, would still be given by Equation (35), but with the following values for the constants:

K_1, as in Equation (36)

K_2, as in Equation (37)

$$C_1 = - \tan \beta \tag{43}$$

$$C_2 = \frac{2}{\sqrt{3}} \bar{\sigma} \tan \beta + \tau + \frac{\bar{\sigma}}{\sqrt{3}} (1 + \tan^2 \beta) \tag{44}$$

τ, as in Equation (40),

and from the geometry of Figure 5b,

$$h' = t + \frac{[h - (h_\ell + t)]}{\tan \alpha} (\tan \alpha + \tan \beta) \tag{45}$$

$$\ell_1 = L - h_\ell / \tan \beta \, . \tag{46}$$

For given die dimensions and for given friction factor, f, the flow model which results in minimum amount of deformation energy or which gives the smallest values for the stress, σ_{yA}, Equation (35) will be valid. Equation (35) can be expressed in dimensionless form by dividing all lengths by the flash thickness, t, to give

$$\frac{\sigma_{yA} - \sigma_{yD}}{\bar{\sigma}/\sqrt{3}} = F\left(f,\ L/t,\ \frac{h_\ell}{t}, \frac{h}{t},\ \alpha,\ \beta\right). \tag{47}$$

Equation (47) was derived from Equations (35) through (46) for the flow models illustrated in Figures 5a and 5b. It is seen, in Equation (47), that the dimensionless increase of the longitudinal stress in the cavity is a function of the die geometry and of the parameters h/t, α, and β. For various values of die with L/t and lower die depth, h_ℓ/t, Equation (47) was minimized to obtain the parameters h/t, α, and β defining the flow model. The results are given in Tables 1 and 2 for two different values of the friction factor, f. The value for theoretical height h_{th} in the tables corresponds to the height of the deformation zone, h, for the case of Figure 4. It is significant to note that, if the flow stress, $\bar{\sigma}$, is assumed to be constant throughout the deformation zone, the location of the flash with respect to upper and lower die surfaces does not influence the increase in longitudinal stress, $\sigma_{yA} - \sigma_{yD}$, in the die cavity. The geometry of the flow model does not vary and consequently the total forging load should not vary significantly with the position of the flash.

The values given in Table 3 were obtained by assigning a 30 percent higher value to the flow stress $\bar{\sigma}$ at the lower die material interface to simulate the increase in flow stress, $\bar{\sigma}$ due to die chilling (for instance steel for 100 C chill). The α, β, and h/t values describing the flow model in Table 3 indicate that the dimensionless stress increase in the die cavity, $\sigma_{yA} - \sigma_{yD}$, becomes slightly larger when compared with the same tool geometry but with lower interface shear-stress τ values (in Table 2). The location of the flash, however, still does not significantly influence the magnitude of the stress in the die cavity.

In the flow model shown in Figure 5c, the height of the deformation zone, h, is determined by die dimensions. The longitudinal stress at the neutral surface, A, is,

$$\sigma_{yA} = \frac{K_2}{K_1} \ln \frac{t}{h'} + \frac{C_2}{C_1} \ln \frac{h'}{h} + 2\tau \frac{\ell_1}{h} + \sigma_{yD}\ , \tag{48}$$

where

σ_{yD} = longitudinal stress at plane D, independent of the parameters α and β

K_1, as in Equation (36)

K_2, as in Equation (37)

C_1, C_2, as in Equations (38) and (39), respectively for $\alpha < \beta$

C_1, C_2, as in Equations (43) and (49), respectively for $\alpha > \beta$

TABLE 1. RELATIONSHIPS BETWEEN DIMENSIONLESS HEIGHT, h/t, AND ANGLES α and β, WHICH DEFINE THE FLOW MODEL FOR GIVEN CAVITY LENGTH, L/t, AND LOWER CAVITY DEPTH, h_ℓ/t, (FRICTION SHEAR STRESS AT LOWER DIE INTERFACE: $\tau = 0.404\ \bar{\sigma}$)

Symbols presented here are illustrated in Figure 5.

L/t	h_ℓ/t	h/t	h_{th}/t	α, degrees	β, degrees	Dimensionless Increase of Stress in Cavity, $\frac{\sigma_{yA} - \sigma_{yD}}{2\bar{\sigma}/\sqrt{3}}$
3.0	0.54	1.62	2.2	35	25	4.66
	0.27	1.54	--	25	25	4.66
	0.14	1.49	--	25	35	4.63
	0.07	1.90	--	25	35	4.65
6.0	1.48	3.44	4.16	35	25	7.24
	0.74	2.69	--	25	35	7.11
	0.37	2.50	--	35	35	7.13
	0.18	2.98	--	35	35	7.24
12.0	3.24	6.51	7.87	35	45	9.88
	1.62	5.21	--	35	45	9.75
	0.81	4.9	--	35	35	9.88
	0.40	5.01	--	35	35	9.99
24.0	6.57	12.17	14.89	35	45	12.56
	3.29	9.49	--	35	45	12.48
	1.64	8.76	--	45	45	12.65
	0.82	11.51	--	45	35	12.89
48.0	12.88	24.18	28.17	45	35	15.28
	6.44	22.19	--	45	45	15.27
	3.22	16.40	--	45	45	15.45
	1.61	21.94	--	45	35	15.71

TABLE 2. RELATIONSHIP BETWEEN DIMENSIONLESS HEIGHT h/t, AND ANGLES α and β, WHICH DEFINE THE FLOW MODEL FOR GIVEN CAVITY LENGTH, L/t, AND LOWER CAVITY DEPTH, h_ℓ/t, (FRICTION SHEAR STRESS AT LOWER DIE INTERFACE: $\tau = 0.577\ \bar{\sigma}$)

Symbols presented here are illustrated in Figure 5.

L/t	h_ℓ/t	h/t	h_{th}/t	α, degrees	β, degrees	Dimensionless Increase of Stress in Cavity, $\frac{\sigma yA - \sigma yD}{2\bar{\sigma}/\sqrt{3}}$
3.0	0.54	1.91	2.2	25	25	5.12
	0.27	1.77	--	25	25	5.11
	0.14	1.68	--	35	25	5.17
	0.07	1.54	--	35	25	5.22
6.0	1.48	3.46	4.16	25	35	7.61
	0.74	3.17	--	35	35	7.61
	0.37	3.12	--	35	25	7.76
	0.18	2.92	--	35	15	7.90
12.0	3.24	6.51	7.87	35	45	10.28
	1.62	5.59	--	35	35	10.27
	0.81	5.26	--	35	25	10.54
	0.40	6.27	--	45	25	10.79
24.0	6.57	12.17	14.89	35	45	12.99
	3.29	10.28	--	35	35	13.06
	1.64	12.38	--	45	35	13.36
	0.82	11.51	--	45	25	13.67
48.0	12.88	22.90	28.17	35	45	15.76
	6.44	22.19	28.17	45	45	15.86
	3.22	23.63	--	45	35	16.17
	1.61	21.94	--	45	35	16.55

TABLE 3. RELATIONSHIPS BETWEEN DIMENSIONLESS HEIGHT, h/t, AND ANGLES α and β, WHICH DEFINE THE FLOW MODEL FOR GIVEN CAVITY LENGTH, L/t, AND LOWER CAVITY DEPTH, h_ℓ/t, (FRICTION SHEAR STRESS AT LOWER DIE INTERFACE: $\tau = 0.577 \times 1.3\ \bar{\sigma}$)

Symbols presented here are illustrated in Figure 5.

L/t	h_ℓ/t	h/t	h_{th}/t	α, degrees	β, degrees	Dimensionless Increase of Stress in Cavity, $\frac{\sigma yA - \sigma yD}{2\bar{\sigma}/\sqrt{3}}$
3.0	0.54	2.09	2.2	25	25	5.41
	0.27	1.9	--	25	15	5.48
	0.14	1.75	--	25	5	5.53
	0.07	1.68	--	25	5	5.65
6.0	1.48	3.95	4.16	35	35	7.94
	0.74	3.51	--	35	25	8.05
	0.37	3.12	--	35	15	8.25
	0.18	2.92	--	35	5	8.39
12.0	3.24	7.48	7.87	35	35	10.57
	1.62	6.11	--	35	25	10.78
	0.81	6.7	--	45	25	11.12
	0.40	6.27	--	45	5	11.39
24.0	6.57	14.15	14.89	35	35	13.31
	3.29	14.1	--	45	35	13.60
	1.64	12.38	--	45	25	13.97
	0.82	11.51	--	45	25	14.40
48.0	12.88	26.76	28.17	35	35	16.11
	6.44	27.01	--	45	35	16.38
	3.22	23.63	--	45	35	16.83
	1.61	21.94	--	45	25	17.38

$$h' = \frac{h_\ell}{\tan \beta} (\tan \alpha + \tan \beta) + t \qquad \text{for } \alpha < \beta \qquad (49a)$$

$$h' = \frac{h_u}{\tan \alpha} (\tan \alpha + \tan \beta) + t \qquad \text{for } \alpha > \beta \qquad (49b)$$

$$\ell_1 = L - \frac{h_u}{\tan \alpha} \qquad \text{for } \alpha < \beta \qquad (50a)$$

$$\ell_1 = L - \frac{h_\ell}{\tan \beta} \qquad \text{for } \alpha > \beta \ . \qquad (50b)$$

Equation (48) can be expressed in dimensionless form to give the dimensionless increase in longitudinal stress:

$$\frac{\sigma_{yA} - \sigma_{yD}}{\bar{\sigma}/\sqrt{3}} = G(f,\ L/t,\ \frac{h_\ell}{t},\ \alpha,\ \beta). \qquad (51a)$$

Equation (51a) corresponds to Equation (47). For given dimensionless cavity length, L/t, lower cavity depth, $\frac{h_\ell}{t}$, and height, $\frac{h}{t}$, and for a given friction factor, f, the angles α and β which minimize the Expression (51) define the geometry of the flow model for those given dimensions. Thus, for a specific application, the function, G, in Equation (51a) must be numerically minimized to obtain the values of α and β that define the flow field. The stresses and the forming loads can then be determined by the derivations given in the Third Interim Topical Report. As a first approximation in estimating α and β, the values given in Tables 1 and 2 can be used. It should be noted that with decreasing value of the friction factor, f, the shear stress over the flat portion of the flow model, Figure 5c, decreases and the material tends to flow in such a way to increase the length of this flat zone. Consequently, for values of $f < 0.3$, the angles α and β both can be estimated to be 45 degrees.

In case the flash line is at the center of the die (refer to Figure 5c), the angles α and β are equal. Equation (51a) transforms into

$$\frac{\sigma_{yA} - \sigma_{yD}}{2\,\sigma/\sqrt{3}} = F = \frac{(1 + \tan^2 \alpha + 2 \tan \alpha)}{2 \tan \alpha} \ln \frac{h}{t} + f\sqrt{3} \left(\frac{L/t}{h/t} - \frac{h/t - 1}{2 \tan \alpha\, h/t} \right). \qquad (51b)$$

Minimizing with respect to $\tan \alpha$

$$\frac{\partial F}{\partial \tan \alpha} = 0 \text{ results in } \tan \alpha_M = \pm \sqrt{\frac{1 - (h/t - 1)\sqrt{3}\, f}{\ln h/t\ (h/t)}} \ . \qquad (51c)$$

Equation (51c) gives the angle, α_M, which should define the flow model for a given friction factor, f. The stresses and loads can then be calculated by using the derivations given in the Third Interim Topical Report.

Flow Models for Formation of a Thick Flash

The determination of a flow model representing the metal flow from a large cavity through a thin flash gap was presented in the Third Interim Topical Report. In the flow model representing the metal flow from a small forging into a fairly thick flash gap, the ratio of the cavity width to flash thickness, L/t, is small. The following condition holds:

$$L/t \leq 2 \tag{52}$$

This condition, Equation (52), was already established in the discussion of metal flow into a smaller cavity, in the Third Interim Topical Report. The discussion presented below applies to plane strain as well as to axisymmetric deformation.

The three possible flow models – I, II, and III – are illustrated in Figures 6a, 6b, and 6c, respectively. Figure 6d illustrates a possible flow model I in longitudinal flow. The material will flow according to the model that results in minimum deformation energy or minimum longitudinal stress, σ_{yA}, at the neutral surface, A. With the present theory based on the slab method of analysis, the flow models I and II, Figures 6a and 6b, can be valid when the angle $\alpha \leq 45$ degrees (i.e., for $L/t \leq 0.5$). When $\alpha > 45$ degrees, the deformation is not upsetting but extrusion and the assumptions of the theory would not hold.

Thus for $L/t \leq 0.5$ and for the possible flow models I and II, σ_{yA} is given by the following equations:

$$\sigma_{yA} = \frac{2\bar{\sigma}}{\sqrt{3}} \left[\frac{1 + \tan^2 \alpha \pm 2 \tan \alpha}{2 \tan \alpha} \right] \ln \frac{t}{h} + 2 \frac{\bar{\sigma}}{\sqrt{3}} \frac{\ell_1}{h} + \sigma_{yC} , \tag{53}$$

where

σ_{yC} = longitudinal stress at the plane, C,

and from the geometry of Figure 6a

$$\ell_1 = L \pm \frac{t - h}{2 \tan \alpha} . \tag{54}$$

Substituting Equation (54) in Equation (53) results in

$$\frac{\sigma_{yA} - \sigma_{yC}}{2\sigma/\sqrt{3}} = \frac{(1 + \tan^2 \alpha \pm 2 \tan \alpha)}{2 \tan \alpha} \ln \frac{t}{h} + \frac{L/t}{h/t} \mp \frac{h/t - 1}{2 \tan \alpha \, h/t} . \tag{55}$$

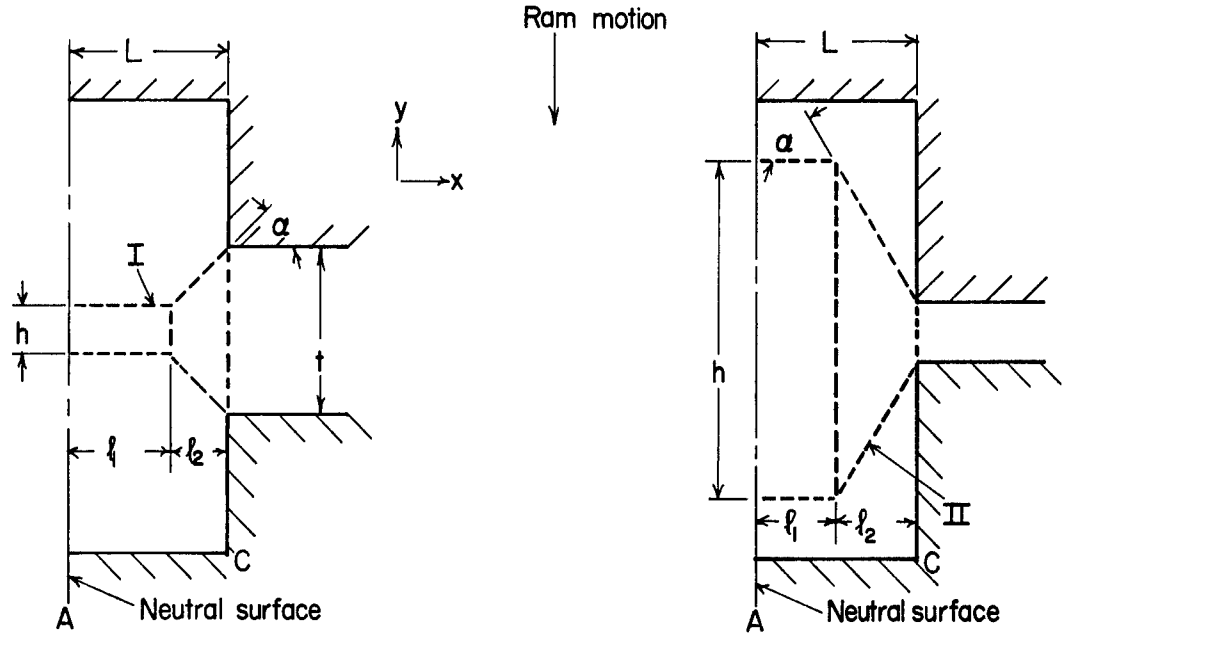

a. Flow Model I, Lateral Flow (Thick Flash)

b. Flow Model II, Lateral Flow (Thin Flash)

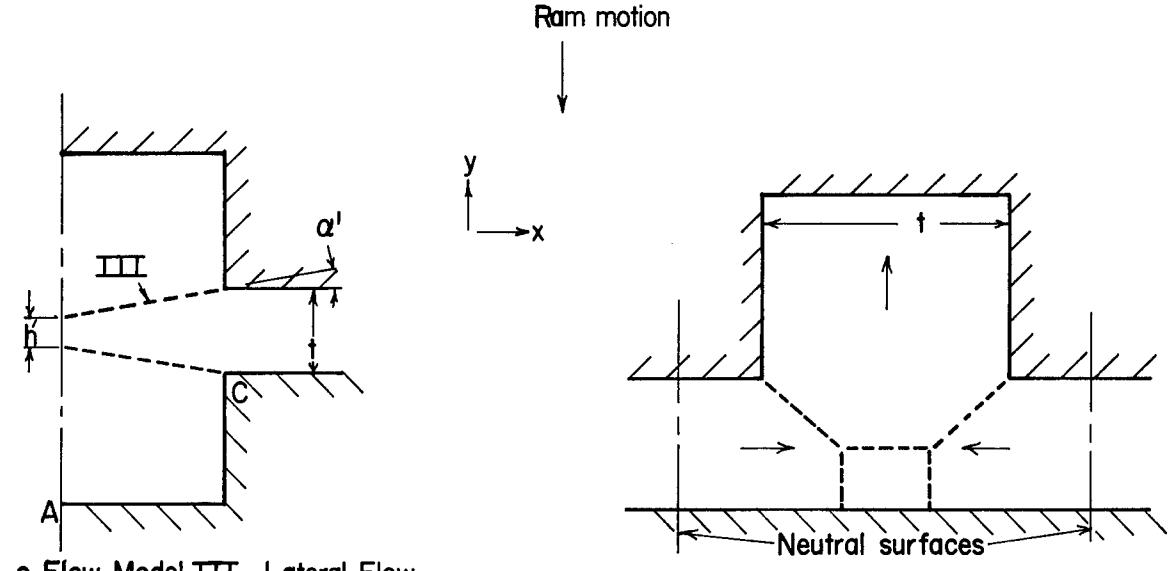

c. Flow Model III, Lateral Flow (Intermediate Flash)

d. Flow Model I in Longitudinal Flow

FIGURE 6. PLANE-STRAIN FLOW MODELS FOR MATERIAL FLOW INTO A FLASH OR CAVITY

Equation (55) expresses the increase in stress between the planes, C, entrance into the die; and A, the neutral plane. It should be noted that Equations (53), (59), and (55) are valid for flow model I (upper algebraic sign) and flow model II (lower algebraic sign) of Figures 6a and 6b. The value of tan α, which results in minimum increase in stress or deformation energy for a given height, h, and which minimizes Equation (55), is obtained from

$$\frac{\partial(\sigma_{yA} - \sigma_{yC})}{\partial \tan \alpha} = 0$$

to give

$$\tan \alpha_M = \left[1 + \frac{(h/t - 1)}{h/t \ln t/h} \right]^{1/2} . \qquad (56)$$

Equation (56) is valid for both flow models I and II of Figures 6a and 6b, where α_M is the angle which minimizes the expression (55). From Equation (56) it is seen that the angle, α_M, depends only on the height, h, of the deformation zone and on the thickness, t, of the flash. The angle, α_M, is independent of the distance, L, between the neutral surface and the die wall as long as the geometry of Figure 6a or 6b exists, i.e., the condition (52), $L/t \leq 2$ holds.

The next unknown to be determined is the height of the deformation zone, h, or the ratio, h/t. One could again minimize the equation (55) with respect to h and the partial derivative:

$$\frac{\partial(\sigma_{yA} - \sigma_{yC})}{\partial h} = 0 \qquad (57)$$

The solution of Equation (57) with Equations (55) and (56) would give the value of height, h. The derivation, however, is very complicated and does not give an explicit expression for the height, h.

The two forms of Equation (55) (with upper and lower algebraic signs) were evaluated for various values of $L/t \geq 0.5$ and for various values of h/t. Equation (56) was used for calculating tan α_M for a given h/t. The values of h/t which minimized Equation (55) are given in Figure 7a where L/t is used as parameter. Figure 7b represents the evaluation of tan α_M from Equation (56) and h/t is determined in Figure 7a.

For $L/t \leq 0.5$ the flow model III of Figure 6c is valid. In this case,

$$h' = t - 2L \tan \alpha' \qquad (58)$$

The increase in longtidutinal stress from plane C to plane A is:

$$\frac{\sigma_{yA} - \sigma_{yC}}{2\sigma/\sqrt{3}} = \left(\frac{1 + \tan^2 \alpha' - 2 \tan \alpha'}{2 \tan \alpha'} \right) \ln \frac{t}{h'} \qquad (59)$$

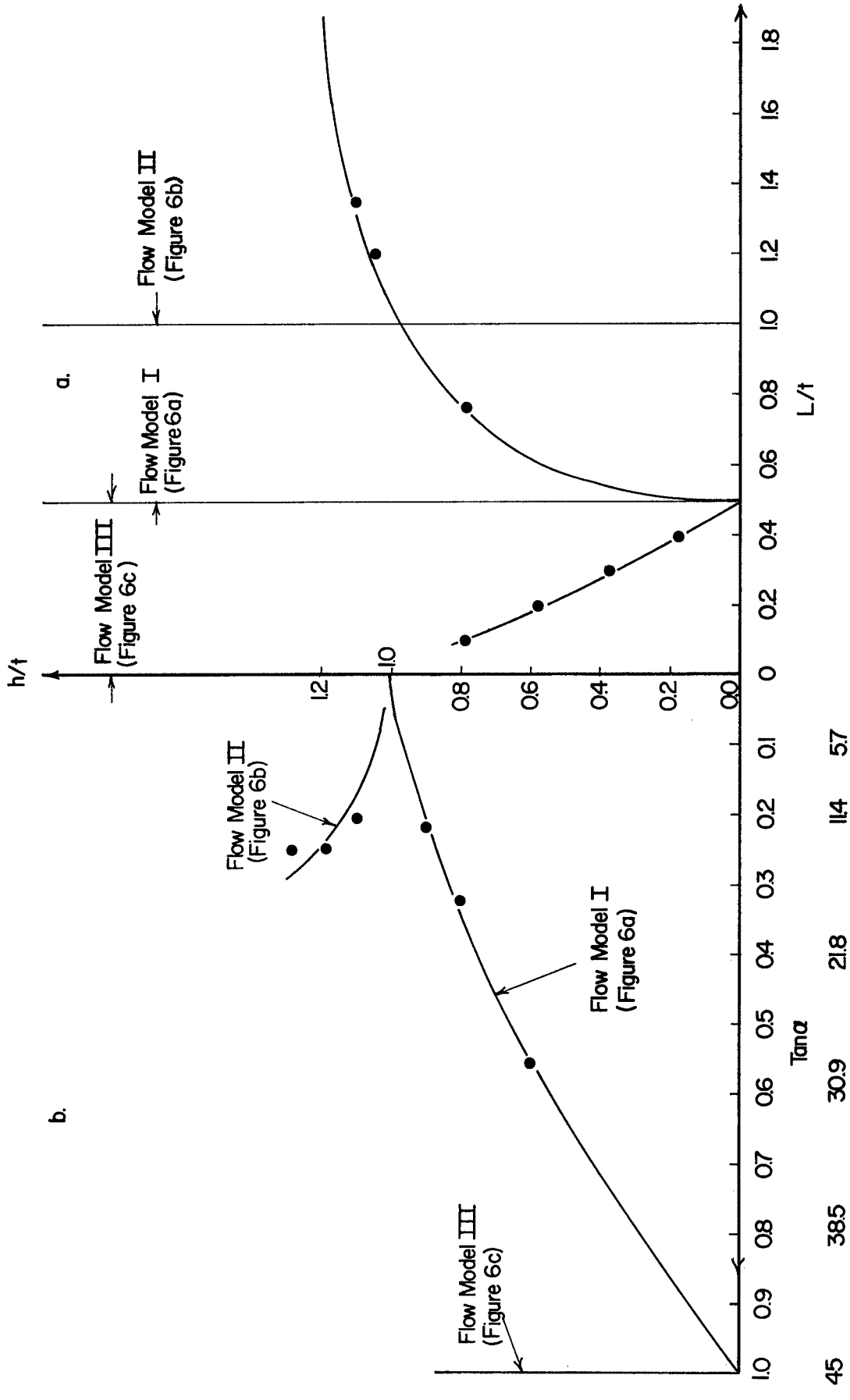

FIGURE 7. DETERMINATIONS OF THE DIMENSIONS FOR THE FLOW MODELS I, II, AND III (FIGURES 6a, 6b, AND 6c) FROM GIVEN VALUES OF DIE-CAVITY LENGTH, L, AND FLASH THICKNESS, t

Using Equation (58), the expression (59) was numerically minimized with respect to tan α' and it was found that for all values of $L/t \leq 0.5$, tan $\alpha' = 1$ or $\alpha' = 45$ degrees gave the minimum values for Equation (59). These results are also incorporated in Figures 7a and 7b, which essentially correspond to the Figure 14 of the Third Interim Topical Report for $L/t \geq 2$.

CONCLUSIONS

The present study is a continuation of the Third Interim Topical Report. The slab method of analysis has been applied to extrusion or filling type metal flow that occurs in closed-die forging.

The flow models discussed in the Third Interim Topical Report have been extended further for more general application. The derivations showed that, after the cavity is completely filled, the location of the flash line has very little effect upon final forging load, provided cooling effects are not very large.

The flow of metal both from thin forgings into flash and from small forgings into larger cavities has been studied in detail. This type of flow is particularly important in the forging of metal into a rib, i.e., in extrusion-type forging.

The theory developed in the third progress report and the present report represent reasonably reliable methods in predicting and analyzing forging mechanics, stresses, and loads. Future work will consist of (1) applying the theory to specific forging operations and (2) studying the heat generation and temperature changes in closed-die forging. A forthcoming report will illustrate the application of the theory developed in the Third and Fourth Interim Topical Reports to practical forging situations.

TA:HJH:AMS/js

LIST OF SYMBOLS

α = angle determining a theoretical flow model

α_M = angle determining the flow model that results in minimum deformation stress

δ = draft angle

f = friction factor in $\tau = f \cdot \bar{\sigma}$, $0 \leqslant f \leqslant 0.577$

γ = draft angle

h = height of a zone in upsetting

h_u = depth of upper die cavity

h_ℓ = depth of lower die cavity

L = distance between neutral surface and die wall

P = forging load over a deformation zone

p = pressure acting perpendicular to tool-material interface

p_u = pressure at upper platen perpendicular to interface

p_ℓ = pressure at lower platen perpendicular to interface

r_o, r_i = outside and inside radii of annular cavity

$\sigma_y, \sigma_x, \sigma_z$ = stress in x, y, z directions, respectively (plane strain)

$\sigma_z, \sigma_r, \sigma_t$ = stress in axial, radial, tangential directions, respectively (axial symmetry)

$\bar{\sigma}$ = effective flow stress assumed to be constant within a deformation zone

τ = friction shear stress at the material-tool interface

t = flash thickness

x = distance from a neutral surface in plane strain forging

w = longitudinal-cavity (shaft) width.